PAPER • OPEN ACCESS

Influence of the magnet aspect ratio on the dynamic stiffness of a rotating superconducting magnetic bearing

To cite this article: Tilo Espenhahn *et al* 2020 *J. Phys. D: Appl. Phys.* **53** 035002

View the article online for updates and enhancements.

Recent citations

- Lateral magnetic stiffness under different parameters in a high-temperature superconductor levitation system*
  Yong Yang and Yun-Yi Wu

- Dynamic Characteristics of a Superconducting Magnetic Bearing Under m Displacements
  Tilo Espenhahn *et al*

- Scalable superconductive magnetic bearing based on non-closed CC tapes windings
  M Osipov *et al*

IOP ebooks™

Bringing together innovative digital publishing with leading authors from the global scientific community.

Start exploring the collection−download the first chapter of every title for free.

Influence of the magnet aspect ratio on the dynamic stiffness of a rotating superconducting magnetic bearing

Tilo Espenhahn[1] ![ORCID]**, Florian Wunderwald**[1,2]**, Marcel Möller**[1,2]**,
Maria Sparing**[1] ![ORCID]**, Mahmud Hossain**[3]**, Günter Fuchs**[1]**, Anwar Abdkader**[3]**,
Chokri Cherif**[3]**, Kornelius Nielsch**[1,2] **and Ruben Hühne**[1] ![ORCID]

[1] Leibniz IFW Dresden, Institute for Metallic Materials, Helmholtzstrasse 20 D-01069 Dresden, Germany
[2] Faculty of Mechanical Engineering, Technische Universität Dresden, Institute for Material Science, TU Dresden, Institut für Werkstoffwissenschaft, D-01062 Dresden, Germany
[3] Faculty of Mechanical Engineering, Technische Universität Dresden, Institute of Textile Machinery and High Performance Material Technology (ITM), Hohe Straße 6, 01069 Dresden, Germany

E-mail: t.espenhahn@ifw-dresden.de

Abstract

Rotating superconducting bearings promise great potential in applications due to their frictionless operation. However, these bearings show a lower dynamic stiffness and damping coefficient compared to ball bearings. In this paper we studied a bearing consisting of a fixed YBCO ring and a rotating magnet above the superconductor. The influence of the magnet aspect ratio on the dynamic stiffness of the bearing was investigated in order to find an optimized size. To change the aspect ratio, we kept the inner diameter of the ring constant and reduced the outer diameter while increasing the ring height. In addition to these magnets, one magnet with a reduced cross-sectional area was studied. The aspect ratio selection was based on preliminary magnetic flux density simulations, which compared the magnetic flux density distribution and the potential radial force for different aspect ratios.

To conduct the measurements, the field-cooled magnets were displaced in a lateral direction and then released, resulting in a damped oscillation. The dynamic stiffness constants were calculated for each bearing from the relation of three axis acceleration measurements for different field cooling heights. The comparison of the stiffness constants for the different bearings revealed an optimal aspect ratio for the given YBCO ring. This optimum is almost independent from the cooling height. The comparison between the two magnet rings with similar diameters and different heights was similar for the bearing characteristics at a low cooling height, whereas a significant reduction of stiffness was observed with a larger cooling distance. The difference is bigger for the magnet with a reduced height. The optimal aspect ratio as well as the stiffness dependence on the cross-sectional area was confirmed by simulations of the magnetic flux density distribution.

Keywords: large scale application, superconducting levitation, rotating bearing, dynamic properties, YBCO

(Some figures may appear in colour only in the online journal)

J. Phys. D: Appl. Phys. **53** (2020) 035002

T Espenhahn *et al*

1. Introduction

Friction and wear have a major influence on the durability of conventional mechanical bearings. In contrast, superconducting bearings (SMB) have the advantage of operating wear-free and with minimal losses. In recent years, SMBs have been studied in a linear configuration for transportation [1–3] or in a rotation-symmetric arrangement as axial or radial bearings for specific applications [4–6]. One example for such a rotation-symmetric configuration is a superconducting magnetic bearing, which was introduced recently by our group in a textile machine as a frictionless replacement for a conventional friction bearing [7, 8]. In this case, the superconducting bearing was made from a fixed $YBa_2Cu_3O_{7-x}$ (YBCO) ring cooled by liquid nitrogen and a free rotating $Nd_2Fe_{14}B$ permanent magnetic ring above the superconductor (figure 1 left) [9]. However, this particular design for a passive rotating superconducting bearing generates a lower dynamic stiffness compared to conventional mechanical bearings. In order to optimize the stiffness for such an application-demanded bearing arrangement, we studied the influence of the magnet aspect ratio on the dynamic stiffness.

The originally used magnet ring for this superconducting magnetic bearing had a height of 6 mm, an inner diameter of 50 mm and an outer diameter of 80 mm. This magnet serves as the starting point for our studies. It should be mentioned that the dynamic properties of the complete system with this particular magnet were previously measured to identify unfavorable operating conditions. However, this study was mainly focused on the rotating speed in order to avoid unfavorable resonance frequencies during operation [10]. In the following, we will focus on the optimization of the stiffness itself for the existing superconductor arrangement in order to reduce the vulnerability of the bearing against exterior disturbances.

2. Method

To change the aspect ratio of the magnet rings we varied the magnet height and the outer diameter while keeping the inner diameter and the magnet cross-sectional area constant. Additionally, one magnet with a reduced cross-sectional area was investigated. The magnets are named according to the outer diameter and the height, i.e. 80×6 for the original magnet with 80 mm outer diameter and 6 mm height (compare table 1). Figure 1 shows the cross section of the different magnets in comparison to the cross section of the superconductor to illustrate the dimension changes. More specifically, the cross section of the original 80×6 magnet is 15 mm $\times$ 6 mm, which results in an aspect ratio of 2.5. The dimensions of the other studied magnets were chosen on the basis of preliminary simulations for the induced magnetic field. In these 2D axial symmetric simulations using the COMSOL software package, the bearing was reduced to the right-handed part of the cross section (compare figure 9) considering the magnet only for its remanence and permeability. All remaining areas were treated as air including the superconductor to determine the magnetic flux density distribution before field cooling. Additionally, the
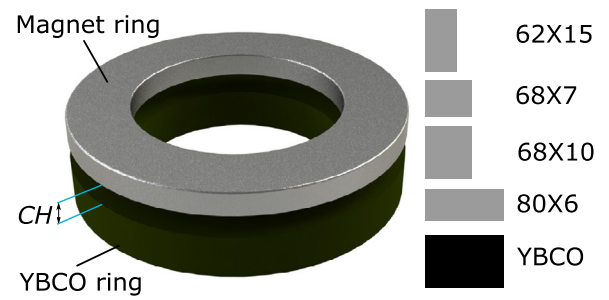

Figure 1. (Left) Schematic setup of the superconducting bearing with the 80×6 magnet. (Right) Comparison of the cross-sectional area between the studied magnets with varying aspect ratio and reduced height.

Table 1. Details of the studied magnet rings in which all magnets had a grade of N45SH ($B_r = 1.33$ T–1.35 T).

| Name | Diameter in mm | | Height in mm | Mass in g | Cross section in mm^2 | Aspect ratio |
	Inner	Outer				
80×6	50	80	6	292	90	2.5
68×10	50	68	10	280	90	0.9
62×15	50	62	15	274	90	0.4
68×7	50	68	7	242	63	1.28

simulated space was surrounded by infinite layers [11] to suppress a flux density increase due to the restricted simulation space.

To compare the different magnet aspect ratios, the force potential for small displacements (F_r) was calculated during simulation for each magnet type. This force potential is based on the Lorenz force and Ampère's law and is defined as the product of the magnetic flux density amplitude B_z and the magnetic flux density gradient inside the superconductor area according to the following formula:

$$F_r = \int_{r_{isc}}^{r_{asc}} \int_{z_{lsc}}^{z_{usc}} B_z * \left(\frac{d(B_z)}{d(r)} - \frac{d(B_r)}{d(z)} \right) \qquad (1)$$

where r_{isc} and r_{asc} are the inner and outer radius and z_{lsc} and z_{usc} are the lower and upper boundaries of the superconductor in the axial direction, respectively. Similar approaches were previously used by other groups to calculate levitation forces; however, such calculations usually include the non-linear conductivity and current density inside the superconductor (see for example [12–14]), which requires significantly higher computational time compared to the simplified approach used here.

In general, we consider only the superconductor area as the bearing characteristics in this design are dominated by the magnetic flux density distribution of the magnet ring in the superconductor cross section. Furthermore, a simplified representation of the superconductor was chosen due to the relatively low flux density value generated by the magnet ring inside the superconductor, which will not push the superconductor into a nonlinear regime.
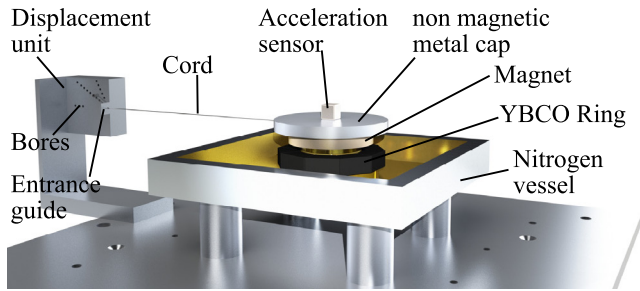
Figure 2. Measurement set up for lateral displacement.

The YBCO-ring consisted of ten single domain segments, which were glued together to a decagon like ring with a maximum outer diameter of 80 mm and an inner diameter of 50 mm [9].

To determine the bearing characteristics, oscillation measurements were performed. Therefore, the permanent magnet is coaxially placed above the YBCO ring at a distance *CH*. Afterwards, the superconductor is field cooled to 77 K. *CH* was varied between 4 mm and 6 mm for all magnets, to study the influence of the cooling height on the dynamic properties. It should be mentioned that the minimal cooling height between the superconductor and the magnet was set to 4 mm due to the cryostat wall, which is placed between both components in a real device setup, i.e. smaller distances would no longer ensure a contact free levitation. On the other hand, cooling heights above 6 mm lead to stiffness values which are too low for using the bearing as a twist element in ring spinning.

For the measurements, a three-axis acceleration sensor (Bruel&Kjær) is placed on top of the levitating magnet above the center using a non-magnetic metal cap (see figure 2). A cord connects the magnet with the displacement unit along the direction of one of the sensors main axes. A guide at the entrance of this unit is used to guarantee a reproducible horizontal pulling of the magnet by the cord in order to minimize the tilting of the magnet otherwise, additional tilting modes would be excited that would make the analysis more difficult as the radial and tilting modes are closely coupled [15].

The cord is fixed with a pin, which is inserted in a bore in the displacement unit. An array of different bores is used in order to realize a constant initial displacement of about 2 mm for all magnets and cooling heights considering that the cord length differs due to its elasticity and the varying stiffness of the bearing. After removing the pin, the magnet snaps back into its equilibrium position. Due to the dynamic properties of the SMB, a damped oscillating movement is generated, which is recorded by the acceleration sensor (figure 3).

The acceleration data of the sensors is processed to determine the bearing characteristics as shown in figure 4. For this analysis, the complete bearing is treated as a mass-spring-damper-system. Therefore, the following steps were performed:

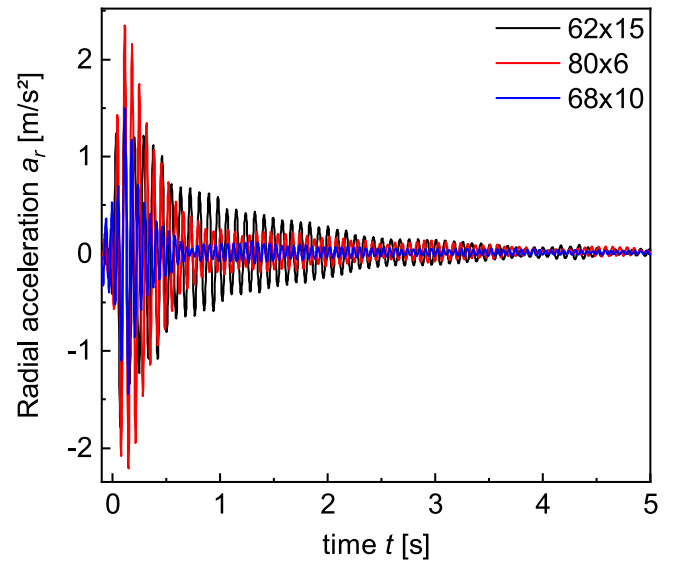1. At first, a peak analysis is completed for the acceleration and position data.

Figure 3. Comparison of the measurement acceleration decay for magnets with the same cross-sectional area. The cooling height was 4 mm.
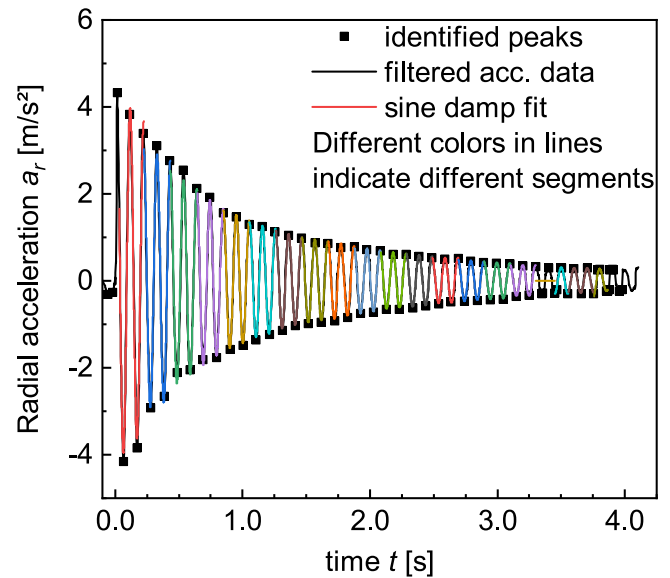

Figure 4. Measurement of the radial acceleration using a 62×15 magnet. The analysis was completed using segmented sine damp fits (see the color code).

2. The magnet oscillation is cut into multiple segments having three maxima and two minima each according to the number of peaks and the corresponding time stamp. This segmentation is conducted to detect any changes in the bearing characteristics for lower displacements.
3. A nonlinear fit is performed for each segment of the acceleration *a* using the function (2) below.
4. The stiffness constant, *k*, for each segment is calculated with the help of function (3)

A damped sine function is used to fit the acceleration data of the magnet:

$$a(t) = a_0 + Ae^{-\delta t} \sin\left(\frac{2\pi * t}{T_d}\right) \qquad (2)$$
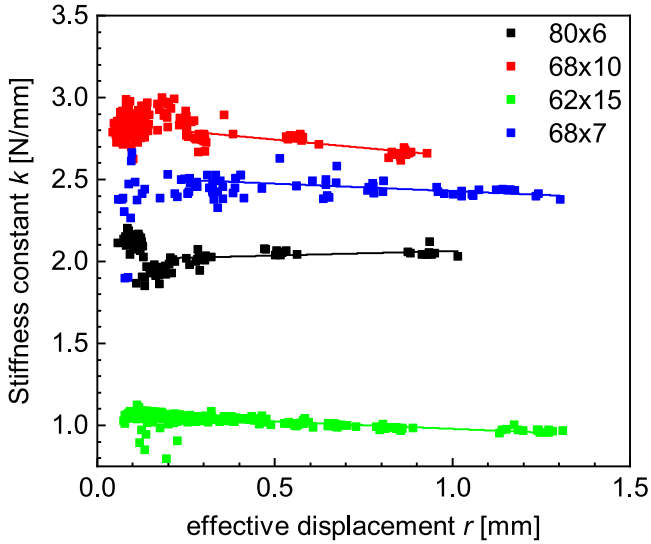
J. Phys. D: Appl. Phys. 53 (2020) 035002

T Espenhahn *et al*

Figure 5. Calculated stiffness constants for multiple measurements with all magnets at a cooling height of 5 mm. Each point represents one segment of a measurement.
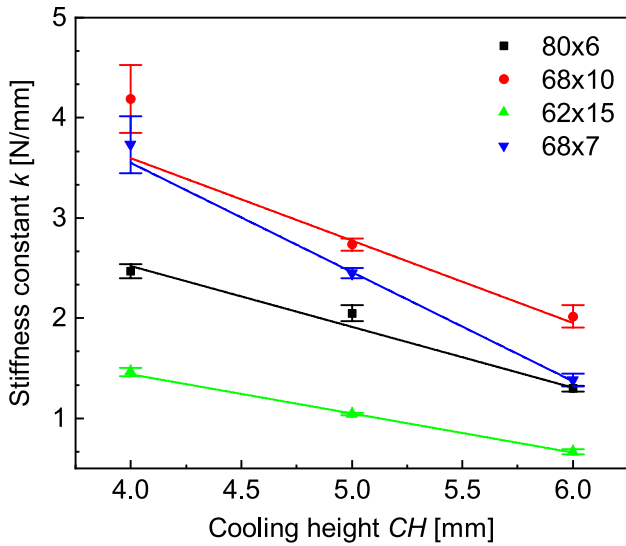

Figure 6. Stiffness coefficients for all magnets at different cooling heights. The error bars result from the scatter in calculated stiffness data (compare figure 5).

Table 2. Stiffness parameters for the different magnets.

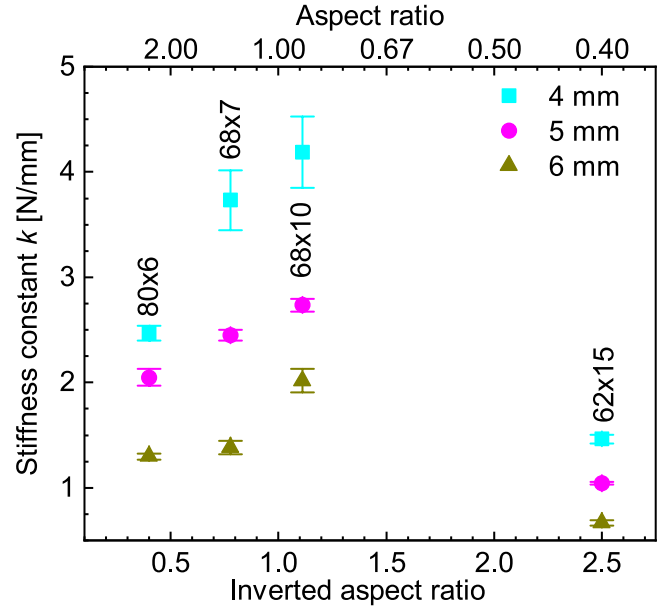| Magnet type	Slope (N/mm)/mm	Stiffness at 4 mm CH (N/mm)
80x6	-607 ± 67	2470 ± 69
68x10	-882 ± 227	4187 ± 339
62x15	-390 ± 14	1462 ± 43
68x7	-1089 ± 54	3733 ± 285

Figure 7. Measured stiffness dependence on the cooling height for magnets with different aspect ratios.

each segment is called the effective displacement and is taken from the peak analysis of displacement data. The displacement is automatically calculated from the acceleration data by the measurement system itself.

The measurement for each magnet type and levitation height was repeated 15 times to reduce the measurement uncertainty.

3. Results and discussion

For comparison, the radial acceleration response is shown in figure 3 for the three magnets with constant cross-sectional area after a similar initial lateral displacement and for the same field cooling distance ($CH = 4$ mm). The data already shows a different damping behavior for the used magnets. In order to quantify the differences, a detailed analysis was performed on the measured data as described above.

Figure 5 depicts all the calculated stiffness values for all magnet types at a cooling height of 5 mm. In general, the stiffness of the superconducting magnetic bearing changes if different magnets are used at the same height over the same YBCO bulk ring. For each magnet the stiffness constant varies only slightly with decreasing effective displacement.

An increased scattering of the stiffness constants was found for an effective displacement below 0.25 mm for all

where δ is the decay constant, T_d the oscillation time period, a_0 a constant offset and A the initial acceleration. All parameters were used for the curve fitting process. The fitting parameters are assumed to be constant within one analysis segment [16], thus no displacement or speed dependency of the fitting parameter is included within one analysis segment. Additionally, the coupling between radial and axial displacements, as well as tilting is neglected.

The dynamic bearing stiffness constant k is calculated from these fitting parameters by:

$$k = m \left(\frac{1}{T_d^2} + \delta^2 \right). \qquad (3)$$

The equation depends on the mass m of the moving magnet, which is given in table 1. The displacement at the beginning of

J. Phys. D: Appl. Phys. **53** (2020) 035002

T Espenhahn *et al*

magnets. This scattering seems to increase with increased mean stiffness. We assume that these changes are related to the increasing influence of external disturbances for the cases with small displacements. This includes the fact that the cord is still connected to the magnet ring after release, vibrations from the exterior that propagate into the system via the nitrogen vessel or even vibrations from the measurements setup itself due to the release procedure. These additional influences can falsify the magnet movement especially at small effective displacements. Due to the data scattering, we limited any further analysis of the data to effective displacement values above 0.25 mm.

The data were used to calculate mean values and standard deviations for the stiffness of the bearing. Figure 6 shows the resulting values for different levitation heights, the slight change of the dynamic stiffness with effective displacement (as shown in figure 5) is included as error bars. The stiffness increases with decreasing levitation height as expected due to increasing magnetic field gradients (compare discussion on figure 9). For the studied cooling heights (i.e. $CH = 4$ mm to 6 mm) this change is almost linear. A comparison between the different magnets indicates that the slimmest magnet (62×15) generates the lowest stiffness followed by the original (80×6) and then the broadest magnet. Between these two extremal cases, the stiffness seems to have a maximum. This observation is valid for all studied cooling heights and can be explained by the magnets pole size and its position relative to the superconductor (see the discussion on figure 9 below).

The dependence of the stiffness on the cooling height is approximated with a linear fit. Table 2 summarizes the calculated slopes of these fits as well as the stiffness at a 4 mm cooling height. It should be mentioned that this linearity works only for the restricted range studied here. Other investigations using a different bearing design found a non-linear stiffness dependence on the cooling height [17, 18]. Restricting the linearity to a small range only might be justified with the non-linear magnetic flux density change over larger distances towards the poles of the ring-shaped permanent magnet [19]. However, for distances or cooling heights comparable to the ones studied here, a nearly linear dependence of the dynamic radial stiffness as well as the flux density change in the axial direction was reported by other groups as well [17, 19].

For the studied magnets with similar cross-sectional areas, the stiffness change and the initial stiffness are linearly correlated. The slope is negative with increasing CH (Pearson correlation coefficient $r = -0.95$). Furthermore, it was found that the higher the stiffness at low levitation height the steeper the stiffness reduction. On the other hand, magnets with a reduced cross-sectional area (i.e. 68×7) show a significantly larger stiffness change compared to the other magnets despite the high stiffness at low cooling height. The main origin for this behavior is the different amount of magnetic material. Whereas the 68×10 magnet belongs to the group of magnets with constant magnetic material, the magnetic material in the case of the 68×7 magnet is reduced due to the reduced height with the same diameter. This reduction of magnetic
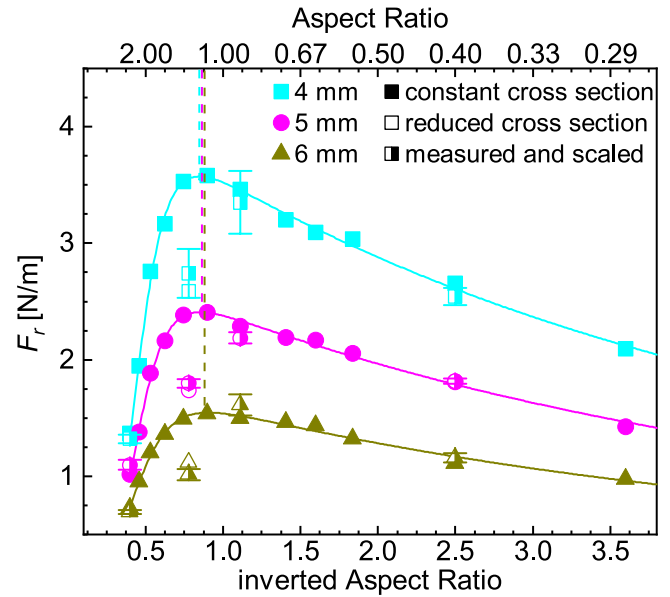

Figure 8. Radial force potential calculated from magnetic flux density simulations. The solid lines are exponential pulse function fits of the data points for each cooling height. The half-filled symbols are the scaled values of the measured data.

material simultaneously influences the magnetic flux density present inside the superconductor and thereby the bearing stiffness constant.

To analyze the stiffness data in more detail, they are plotted over the aspect ratio of the magnet versus a constant cooling height (figure 7). The data suggest the existence of an optimal aspect ratio for all studied levitation heights, which is independent from CH itself. This result indicates that the magnet dimension dominates the behavior. Comparing the different aspect ratios, it is obvious that the 68×10 magnet generates the highest dynamic stiffness for all cooling heights. The origin for this dependence might be the difference in magnet pole size and magnetic material utilization between the three magnets and will be discussed in the following.

To support the previous assumption, figure 9 compares the simulated magnetic flux density distribution in the cross-section view for all magnets studied here. For all three subfigures, only half of the ring is shown. The superconductor section area is marked with a box below the magnets for comparison. For all subfigures the same color scale for the magnetic flux density was used. It should be mentioned that the simulation procedure included infinite subdomains at the outer boundaries of the air subdomain to suppress the magnetic feedback from a too narrow air subdomain.

Comparing the three subfigures for the magnets with the same cross-sectional area, one can identify that the material utilization is best for the 62×15 magnet (figure 9(c)), i.e. the flux density inside this magnet is highest. This leads to a high flux density over the complete magnet pole width. However, due to the relatively slim pole (i.e. the distance between the inner and outer edge) the high flux density is only present in a smaller part of the superconductor. Therefore, only small restoring forces and radial stiffness can be generated.
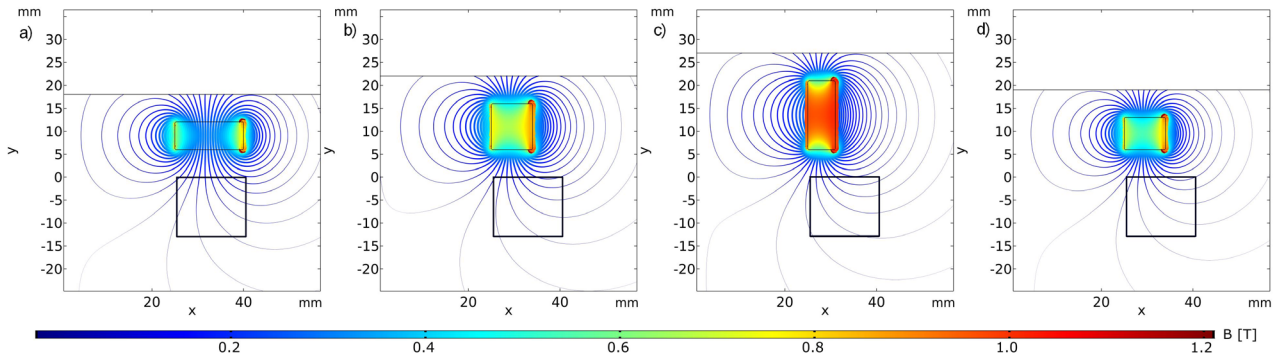
Figure 9. Comparison of the generated magnetic flux density distribution for different magnets (a) 80×6 (b) 68×10, (c) 62×15 and (d) 68×7. The position of the superconductor is marked with a black box. The magnetic flux density along the flux lines is indicated by the thickness as well as the color of the flux line.

The 80×6 magnet shows a completely different behavior. Here, the material utilization is relatively low resulting in a significantly larger magnetic pole size with a lower magnetic flux density. However, this low flux density is active in a larger region of the superconductor below and therefore results in a higher stiffness compared to the 62×15 magnet. Furthermore, areas with high magnetic flux density are only present at the edge of the superconductor and are therefore only active inside the superconductor for either positive (inner edge) or negative (outer edge) radial displacements. The 68×10 magnet is the best trade-off between these two extrema. Nevertheless, a flux density reduction along the bottom edge is already visible for the 68×10 magnet, which is indicated by the color change along the magnet bottom line.

It is also possible to quantify the influence of the aspect ratio based on these simulations by comparing the force generation of the different magnets (F_r as explained in the Methods section). Therefore, the product of magnetic flux density in the axial direction with the difference of the flux density gradient in the axial and radial directions is integrated over the superconducting region.

Figure 8 shows the results for different magnet aspect ratios at a levitation height of 4 mm, 5 mm and 6 mm. The simulation allows for the determination of an optimal aspect ratio, because more aspect ratios were simulated than measured (fully filled symbols). It is apparent that the dependence of the force on the aspect ratio follows an exponential pulse function. This behavior is due to the fact that the inner diameter remains constant, resulting in an asymmetry of the magnet above the superconductor for smaller outer diameters. Additionally, two effects contribute to the force change. On one hand, the flux density applied to the superconductor increases with decreasing aspect ratio. On the other hand, the area in which the increased flux density is active inside the superconductor decreases with increasing aspect ratio. For aspect ratios above 1.2 the effect of increasing flux density dominates. For aspect ratios below 1 the reduction of the active area dominates the levitation force, as the magnetic flux density reaches saturation and cannot be increased above 0.6 T at the magnets surface. Fitting the simulation data with an exponential pulse

function leads to the solid lines plotted in figure 8. As a result, the optimal radial force is found for an aspect ratio between 1.10 and 1.17. The difference of the simulated optimal aspect ratios for different cooling heights is within the error of regression (aspect ratio $\pm$ 0.085). Additionally, the measured data points are included in figure 8 (half filled symbols). The measured data points were scaled with a constant factor for each magnet to compensate for the assumptions made for the simulation (i.e. the application of a non-dynamic simulation). It can be seen that the measured data points are in good agreement with the corresponding simulated data points at the specific aspect ratios. Therefore, the resulting simulated optimum can be transferred to the measurements.

Figure 8 also includes the simulation data of the 68×7 magnet with reduced cross section area for a levitation height of 4 mm, 5 mm and 6 mm, respectively (empty symbols). The simulation shows a similar trend as the measurement data. As expected, the simulated as well as the measured forces of the magnet with reduced section area are lower for all levitation heights.

4. Conclusion

The dynamic stiffness of a rotating superconducting magnetic bearing was studied for their dependence on the aspect ratio of the magnet. Three magnets with different aspect ratios but constant cross-sectional area as well as one magnet with a reduced cross-section were studied. For all four magnets the same YBCO ring was used.

While changing the aspect ratio, an optimal aspect ratio with highest dynamic stiffness was found. This optimal aspect ratio is independent of the cooling height, which was studied in a range between 4 mm and 6 mm. The optimal solution is a magnet with a pole width smaller than the superconductor width. Reducing the magnet height while keeping the pole width constant leads to a reduced stiffness at higher cooling heights and similar stiffness at low cooling heights. Simulations of the magnetic flux distribution confirmed the measurements and allowed us to understand the relations between the magnet material utilization and the pole width.

J. Phys. D: Appl. Phys. **53** (2020) 035002

T Espenhahn *et al*

Acknowledgments

ORCID iDs

Tilo Espenhahn ⓘ https://orcid.org/0000-0002-7621-8810
Maria Sparing ⓘ https://orcid.org/0000-0003-1653-048X
Ruben Hühne ⓘ https://orcid.org/0000-0002-0030-6048

References

[1] Deng Z *et al* 2016 A high-temperature superconducting maglev ring test line developed in Chengdu, China *IEEE Trans. Appl. Supercond.* **26** 3602408

[2] Schultz L *et al* 2005 Superconductively levitated transport system—the SupraTrans project *IEEE Trans. Appl. Supercond.* **15** 2301–5

[3] Sotelo G G, de Oliveira R A H, Costa F S, Dias D H N, de Andrade R and Stephan R M 2015 A full scale superconducting magnetic levitation (MagLev) vehicle operational line *IEEE Trans. Appl. Supercond.* **25** 3601005

[4] Arsenio A J, Vaz de Carvalho M d L M, Cardeira C, Melicio R and Costa Branco P J 2017 Experimental setup and efficiency evaluation of zero-field-cooled (ZFC) YBCO magnetic bearings *IEEE Trans. Appl. Supercond.* **27** 3601105

[5] Hekmati A, Hekmati R and Siamaki M 2017 Proposed design for superconducting magnetic bearing system with high-temperature superconducting discs *IEEE Trans. Appl. Supercond.* **27** 5204408

[6] Yu Z, Zhang G M, Qiu Q, Hu L, Zhuang B and Qiu M 2014 Analyses and tests of HTS bearing for flywheel energy system *IEEE Trans. Appl. Supercond.* **24** 5700405

[7] Sparing M *et al* 2015 Superconducting magnetic bearing as twist element in textile machines *IEEE Trans. Appl. Supercond.* **25** 3600504

[8] Hossain M *et al* 2014 Innovative twisting mechanism based on superconducting technology in a ring-spinning system *Text. Res. J.* **84** 871–80

[9] Berger A *et al* 2016 Cryogenic system for the integration of a ring-shaped SMB in a ring-spinning tester *IEEE Trans. Appl. Supercond.* **26** 3601105

[10] Sparing M *et al* 2016 Dynamics of rotating superconducting magnetic bearings in ring spinning *IEEE Trans. Appl. Supercond.* **26** 3600804

[11] Beer G and Meek J L 1981 'Infinite domain' elements *Int. J. Numer. Methods Eng.* **17** 43–52

[12] Zheng J, Huang H, Zhang S and Deng Z 2018 A general method to simulate the electromagnetic characteristics of HTS Maglev systems by finite element software *IEEE Trans. Appl. Supercond.* **28** 3600808

[13] Hong Z, Campbell A M and Coombs T A 2006 Numerical solution of critical state in superconductivity by finite element software *Supercond. Sci. Technol.* **19** 1246–52

[14] Dias D H N *et al* 2009 Simulations and tests of superconducting linear bearings for a MAGLEV prototype *IEEE Trans. Appl. Supercond.* **19** 2120–3

[15] Cansiz A 2009 Vertical, radial and drag force analysis of superconducting magnetic bearings *Supercond. Sci. Technol.* **22** 075003

[16] Motta E S, Dias D H N, Sotelo G G and Stephan R M 2013 Dynamic tests of an optimized linear superconducting levitation system *IEEE Trans. Appl. Supercond.* **23** 3600504

[17] Cansiz A, Hull J R and Gundogdu Ö 2005 Translational and rotational dynamic analysis of a superconducting levitation system *Supercond. Sci. Technol.* **18** 990–6

[18] Cansiz A 2003 Correlation between free oscillation frequency and stiffness in high temperature superconducting bearings *Physica* C **390** 356–62

[19] Smolyak B M and Zakharov M S 2014 On the force relaxation in the magnetic levitation system with a high-T_c superconductor *Supercond. Sci. Technol.* **27** 055018